Neural Networks 181 (2025) 106888

Contents lists available at ScienceDirect

Neural Networks

journal homepage: www.elsevier.com/locate/neunet

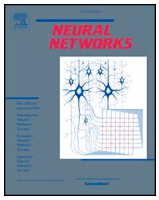

Full Length Article

Dopamine-induced relaxation of spike synchrony diversifies burst patterns in cultured hippocampal networks

Huu Hoang [a,*], Nobuyoshi Matsumoto [b,c], Miyuki Miyano [b,c], Yuji Ikegaya [b,c,d,*], Aurelio Cortese [e,*]

[a] Neural Information Analysis Laboratories, ATR Institute International, 619-0288 Kyoto, Japan
[b] Graduate School of Pharmaceutical Sciences, The University of Tokyo, 113-0033 Tokyo, Japan
[c] Institute for AI and Beyond, The University of Tokyo, 100-0005 Tokyo, Japan
[d] Center for Information and Neural Networks, National Institute of Information and Communications Technology, 565-0871 Osaka, Japan
[e] Computational Neuroscience Laboratories, ATR Institute International, 619-0288 Kyoto, Japan

ARTICLE INFO

Keywords:
Dopamine
Cultured hippocampus
Burst dynamics
Network analysis

ABSTRACT

The intricate interplay of neurotransmitters orchestrates a symphony of neural activity in the hippocampus, with dopamine emerging as a key conductor in this complex ensemble. Despite numerous studies uncovering the cellular mechanisms of dopamine, its influence on hippocampal neural networks remains elusive. Combining in vitro electrophysiological recordings of rat embryonic hippocampal neurons, pharmacological interventions, and computational analyses of spike trains, we found that dopamine induces a relaxation in network synchrony. This relaxation expands the repertoire of burst dynamics within these hippocampal networks, a phenomenon notably absent under the administration of dopamine antagonists. Our study provides a thorough understanding of how dopamine signaling influences the formation of functional networks among hippocampal neurons.

Introduction

The brain operates as a dynamic and intricately interconnected network of neurons, where neurotransmitters choreograph the symphony of neural activity (Bullmore & Sporns, 2009; Friston, 2011). Among these neurotransmitters, dopamine (DA) emerges as a central orchestrator, exerting profound effects across various brain regions (Wise, 2004; Schultz, 2007). Notably, the hippocampus stands out as a significant target of dopaminergic influence, receiving inputs from multiple brain nuclei (Swanson, 1982; Gasbarri et al., 1997; McNamara & Dupret, 2017; Takeuchi et al., 2016). The indispensable role of dopamine in hippocampal function is evident from previous research emphasising its involvement in spatial navigation (Xing et al., 2010; Kempadoo et al., 2016), memory formation (Shohamy & Adcock, 2010; da Silva et al., 2012) and even neuropsychiatric disorders such as schizophrenia (Grace, 2012, 2016).

In vitro cell cultures, combined with multi-electrode arrays (Kayama et al., 2018; Sasaki et al., 2019), offer compelling models for investigating neuronal activity in the hippocampus under the influence of dopamine. Previous studies have demonstrated that in vitro hippocampal neurons exhibit characteristic network-wide bursting activity (Suresh, 2016; Gonzalez-Sulser et al., 2012; Mody & Staley, 1994; Pimashkin et al., 2011). This activity can be experimentally manipulated by modulating synaptic transmission (Niedringhaus et al., 2013) or influencing dopamine-receptor sensitivities (Xie et al., 2011; Miyawaki et al., 2014; Li et al., 2017). Despite these insights into its cellular mechanisms (Yamada et al., 2002; Zhang et al., 2009), there is a significant gap in understanding how dopamine impacts hippocampal network-level activity, which is critical for understanding the hippocampus's role in learning, memory, and spatial navigation (Lisman, 2011; McNamara et al., 2014; Lisman et al., 2011). In the present study, we systematically explored the relationship between dopamine-induced alterations in network synchrony and the subsequent changes of burst patterns in primary hippocampal cultures. Employing a comprehensive approach involving electrophysiological recordings, pharmacological interventions, and computational analyses, we unveiled that dopamine induces a relaxation of synchrony within hippocampal networks, an effect characterised by a reduction in spike coherence in 1-msec bins. This relaxed state facilitates the emergence of a broader range of burst patterns within the neuronal ensemble, distinguished by clusters of

* Corresponding authors.
E-mail addresses: hoang@atr.jp (H. Hoang), yuji@ikegaya.jp (Y. Ikegaya), cortese.aurelio@gmail.com (A. Cortese).

https://doi.org/10.1016/j.neunet.2024.106888
Received 9 July 2024; Received in revised form 17 October 2024; Accepted 31 October 2024
Available online 7 November 2024

rapid firing interspersed with periods of relative quiescence. In addition, we demonstrated that dopamine-induced changes in network synchrony correlate with the diversification of burst patterns, a correlation absent in samples treated with dopamine antagonists. These results suggest that dopamine plays a crucial function in shaping neural representations within the hippocampus, influencing information encoding, storage, and retrieval. Our study provides novel insights into the fundamental principles governing hippocampal information processing by dissecting the underlying mechanisms governing these phenomena.

Results

We prepared a total of eight primary cultures from rat embryonic hippocampus and used MaxOne high-density microelectrode arrays (MaxWell Biosystems, Switzerland) to capture spiking activity across several hundred active electrodes (Table 1). Initially, spikes were recorded in the absence of dopamine in the bath and were considered as the baseline condition. Subsequently, dopamine (DA) was gradually introduced into the bath, and spike recording sessions were conducted (Fig. 1A). We systematically examined the effect of DA concentration on firing rate and found that dopamine concentrations ranging from 30 to 1000 μM consistently elevated the firing rate compared to baseline, in agreement with previous studies (Behr et al., 2000; Weiss et al., 2003). Consequently, in this study we analysed the effects of dopamine within this concentration range (see Supplementary Fig S1). A linear mixed-effect model (see Methods for details) indicated that the neurons' firing rate increased in response to the effects of dopamine (mean ± *s*.e.m of the mean firing rate, 1.6 ± 0.3 Hz, 1.7 ± 0.3 Hz, 1.9 ± 0.4 Hz, 2.0 ± 0.3 Hz, 2.4 ± 0.3 Hz for baseline, 30, 100, 300, 1000 μM DA conditions, respectively; linear mixed-effects model, mean ± *s*.e.m of DA coefficient, 0.24 ± 0.05, $p < 0.00001$). Examination of the raster plots of a representative sample revealed spontaneous, highly synchronised spikes, forming bursts within a 200–300 ms timeframe (Fig. 1B). The presence of spike bursts, even evident under baseline conditions, implies the potential existence of neuronal networks influencing spiking dynamics within hippocampal cultures (Pimashkin et al., 2011; Suresh et al. 2016). In the following sections, we investigated the impact of dopamine on network synchrony and its subsequent effects on bursting patterns. Each analysis began with an examination of the effects on a representative sample, followed by group-level results and statistics.

Dopamine reduces spike synchrony in hippocampal networks

To analyze the networks in hippocampal cultures, we assumed that the connectivity between the electrodes could be represented by their temporal coherence. Consequently, we constructed a synchrony matrix for each sample under a specific condition. Each row and column in the synchrony matrix correspond to individual electrodes, and the value indicates the synchrony strength, quantified as spike coherence in 1 msec bins (Fig. 2A, see Methods for details). Comparing two conditions (baseline and 1000 μM, Fig. 2B and C) in the representative sample revealed a notable reduction in synchrony strength between electrode pairs in the presence of DA (mean ± std of synchrony strength across electrode pairs, 0.04 ± 0.04 and 0.02 ± 0.03 for baseline and 1000 μM, respectively, Fig. 2D). This reduction was consistent across all electrode pairs (Fig. 2E), suggesting that dopamine broadly impacted network synchrony.

Table 1
Summary of the data samples. Values in columns of # active electrodes and DIV indicate mean ± *s*.e.m across samples. DIV – day in vitro.

Sample group	# samples	# active electrodes	DIV
No-Antagonist	8	768 ± 94	61.2 ± 38.7
SCH23390 (10 μM)	9	800 ± 30	57.8 ± 15.7
Sulpiride (100 μM)	12	756 ± 112	50.2 ± 11.3

Considering all samples, synchrony strength consistently diminished with increasing dopamine concentration levels. A linear mixed-effects model with the mean synchrony strength as the response variable captured this effect, showing a negative coefficient of DA concentration level (mean ± *s*.e.m, −0.0013 ± 0.0004, $p = 0.006$). Post-hoc tests highlighted that, relative to baseline, the reduction in synchrony strength was statistically significant for all dopamine conditions except the 30 μM condition (mean ± *s*.e.m of % change in the mean synchrony strength across samples: −3 ± 2%, −7 ± 3%, −7 ± 3%, −12 ± 6% for 30, 100, 300, 1000 μM DA conditions, respectively, Fig. 2E). Importantly, highlighting its robustness, this trend was observed irrespective of bin size (Supplementary Fig S3D, varying bin size from 1 to 50 msec).

Dopamine increases the number of network modules and confines the connectivity within individual modules

In our study, we delved into the organisation of hippocampal networks in terms of distinct modules, each potentially responsible for specific aspects of computation or learning. To this end, we conducted modularity analyses of the synchrony matrix, aiming to identify a limited number of modules characterised by significantly stronger synchrony within modules compared to that across modules (see Methods for details). Analysing the representative sample revealed three key observations when comparing the modules detected in the baseline condition with those under 1000 μM DA condition (Fig. 3A–C). First, the modules were non-overlapping localised regions within the network (Fig. 3A). Second, while two out of three modules in the baseline condition retained their structure, one module (depicted by purple dots in Fig. 3A) was split into two distinct modules when exposed to 1000 μM DA concentration (indicated by purple and green dots in Fig. 3B). Third, electrodes exhibited a higher likelihood of connectivity with other within-module electrodes under the 1000 μM DA condition compared to the baseline, as evidenced by the smaller number of across-module connections (black thick traces in Fig. 3A and B). This was corroborated by the participation coefficient, a metric that quantifies the strength of connections between electrodes within their respective modules (see Methods for details), with higher coefficients indicating greater within-module connections (mean ± std of participation coefficient across electrodes, 0.55 ± 0.08, 0.62 ± 0.08 for Non and 1000 μM DA conditions, respectively, Fig. 3C).

All of these observations held true upon systematic examination across all samples. Specifically, the distance between electrodes within a module (~800 μm) was approximately half of that across modules (>1700 μm), and these distances remained unchanged even under the influence of dopamine (Fig. 3D), suggesting spatial confinement of the modules. Linear mixed-effects models revealed that elevated dopamine concentrations correlated with an increase in both the number of modules and participation coefficients (mean ± *s*.e.m of DA coefficient across samples, 0.24 ± 0.10, $p = 0.016$ for number of modules and 0.03 ± 0.01, $p = 0.0015$ for participation coefficients). Relative to the baseline level, the number of modules exhibited a percentage change of 9 ± 7%, 27 ± 14%, 19 ± 8%, 19 ± 7% for 30, 100, 300, and 1000 μM DA conditions, respectively (Fig. 3E). Similarly, participation coefficients displayed a percentage change of 7 ± 4%, 11 ± 6%, 17 ± 8%, 19 ± 9% for 30, 100, 300, 1000 μM DA conditions, respectively (Fig. 3F). These increases were notably significant when dopamine concentrations ranged from 100 to 1000 μM.

Dopamine diversifies activation patterns in burst events

We next sought to understand how dopamine would lead to alterations in spike dynamics. To address this question, we focused on the activation patterns of bursts for two main reasons. First, the networks exhibited bursting events characterised by high-frequency spiking involving a large number of electrodes (Fig. 1B). Second, previous studies have indicated that the delays between the initial spikes within

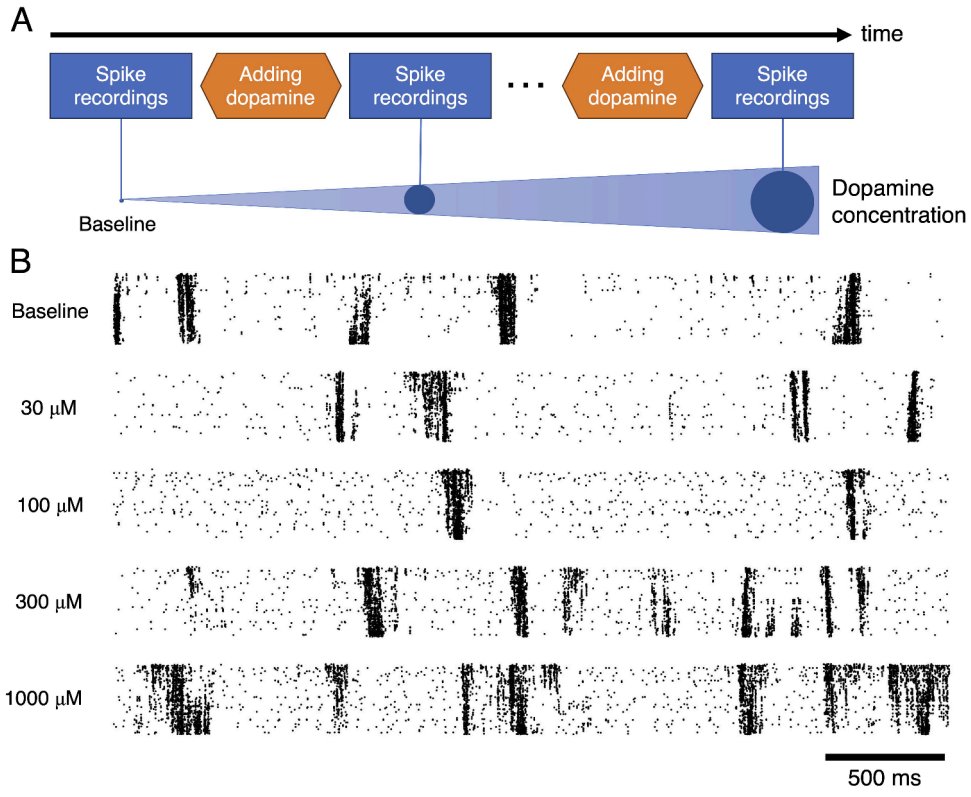

Fig. 1. Dopamine experiment on hippocampal cultures recorded by MaxOne Chip.
A: The experimental scheme. Spike recordings were conducted at baseline, and each time dopamine was added to the bath. B: Raster plots depicting spiking activity of active electrodes for the representative sample at baseline level (top) and at four levels of dopamine (DA) concentration (second to bottom, 30, 100, 300, 1000 μM). Note that we used this representative sample to illustrate subsequent analyses (see Figs. 2-4).

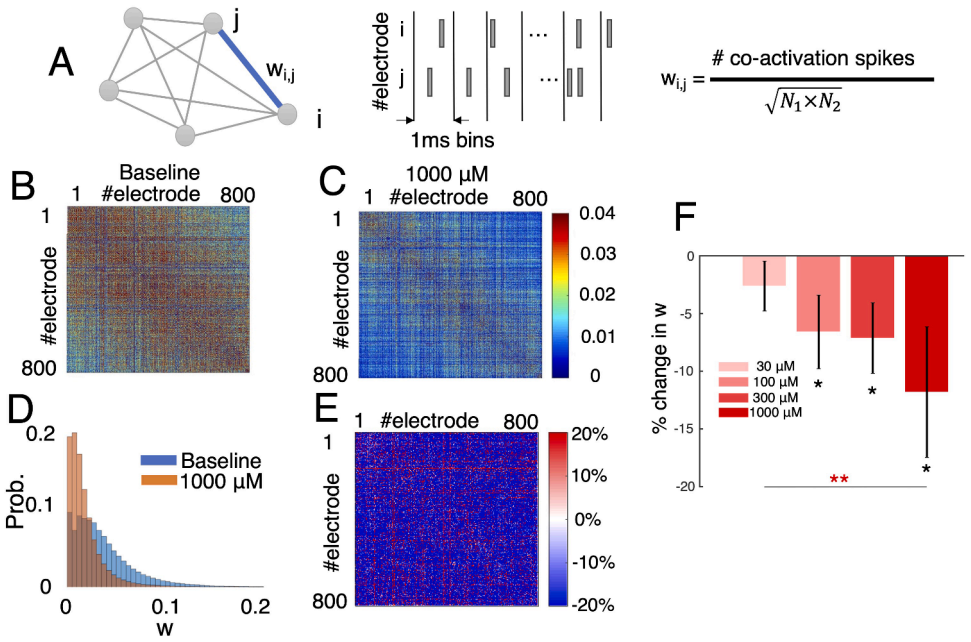

Fig. 2. Effects of dopamine on synchrony strength of hippocampal networks.
*A: Network analysis with the synchrony strength defined as co-activation of spikes within 1-msec bins. B-E: Synchrony matrix of the representative sample in the baseline condition (B) and when the DA concentration level reached 1000 μM (C), histograms of synchrony strength (D), and difference in synchrony matrix (E). F: Change in averaged synchrony strength, compared to the baseline level, for the four DA conditions (four shades of red, each for 30, 100, 300, 1000 μM) in n = 8 samples. Bars with errors represent mean and s.e.m, respectively. Red asterisks indicate the significance level of the main effect of DA, computed with a linear mixed effects model. Black asterisks indicate the significance level of one-tailed t-tests against 0. * $p < 0.05$, ** $p < 0.01$.*

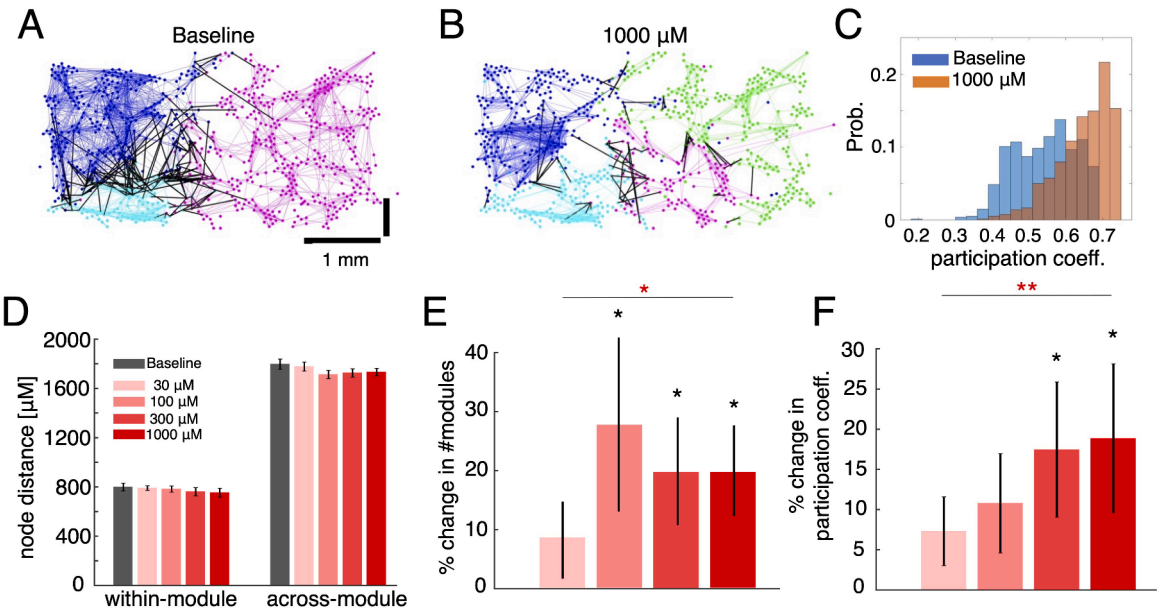

Fig. 3. Effects of dopamine on network clusters and their synchrony.
A-B: Spatial profiles of the representative sample in the baseline condition (A) and 1000 μM condition (B). Each dot represents the relative position of a single electrode in the MaxOne high-density microelectrode array. Colors represent the modularity, where electrodes in the same module share the same color. Lines connect the electrode pairs whose synchrony strength was greater than a threshold, defined by the top 1% in the baseline condition. Colored thin lines connect electrodes in the same module and black thick lines connect electrodes in different modules. C: Histograms of participation coefficients of the electrodes in the baseline condition (blue bars) and 1000 μM condition (orange bars) for the representative sample. D: Distance of electrode pairs in the two pools of within-module and across-module for the baseline condition (grey bars) and the four DA conditions (red shaded bars). E-F: Changes in number of modules (E) and the mean participation coefficient (F), normalized by the baseline level, for the four DA conditions, n = 8 samples. The convention was the same as in Fig. 2.

bursts of individual electrodes (activation patterns) reflect functional connectivity that remains relatively stable on the timescale of 100–200 ms (Raichman & Ben-Jacob, 2008; Pimashkin et al., 2011). Hence, we adopted a similar approach to Raichman and Ben-Jacob (2008) to quantitatively assess the changes in activation patterns across bursts induced by dopamine (see Methods for details).

Initially, bursts were detected by applying a threshold (0.2 standard deviations) to the trace of the number of active electrodes counted in 10-ms bins (Fig. 4A). For each burst, the activation pattern was represented by a matrix A, where $A(i,j)$ denotes the delays in milliseconds between the first spike of the i-th electrode and the first spike of the j-th electrode (Fig. 4B). Our investigation indicated that the bursts endured for roughly 200 msec (mean ± s.e.m, 204 ± 15 msec) with a firing rate of about 9 Hz (mean ± s.e.m, 8.8 ± 0.4 Hz) and exhibited no notable change in either duration or burst firing rate under the influence of dopamine (data not shown). Note that the detected bursts remained consistent despite variations in the two parameters, threshold and bin size (Supplementary Fig S3A-B).

We then measured the similarity index between two bursts as the fraction of electrode pairs (i,j), whose difference in $A(i,j)$ of the two bursts is less than a temporal window of 50 msec. The similarity matrix was constructed by comparing the activation patterns between all detected bursts (Fig. 4C). Next, we applied the affinity propagation algorithm on the similarity matrix to identify the repeating motifs–burst patterns that occur frequently within the data–offering insights into underlying burst dynamics (see Methods for details). For the representative sample, we found that 1000 μM DA concentration increased the number of bursts 4-folds and the number of repeating motifs 3-folds, and significantly reduced the similarity index in their activation patterns (mean ± std of similarity index, 0.11 ± 0.10, 0.02 ± 0.03 for baseline and 1000 μM condition, respectively, Fig. 4C–F). Interestingly, the electrodes were co-activated within short temporal windows of <100 msec in the baseline condition (Fig. 4G), but such activation was temporally and spatially divergent under the influence of dopamine (Fig. 4H). Note that the change in bursting events was temporally irrelevant, both in the baseline and dopamine conditions (Supplementary Fig. S5).

Examination across eight samples confirmed that elevated DA concentrations increased the number of bursts (linear mixed-effects model with the number of bursts as response variable, mean ± s.e.m of DA coefficient, 47.5 ± 15.4, $p = 0.003$; mean ± s.e.m of % change in number of bursts relative to baseline level, 49 ± 43%, 70 ± 51%, 115 ± 83%, 161 ± 86% for 30, 100, 300, 1000 μM DA conditions, respectively, Fig. 5A). In contrast, increased concentrations of dopamine led to a decrease in the mean similarity index between bursts. This was evidenced by a linear mixed-effects model with the mean similarity index as the response variable showing a negative coefficient of DA concentration level (mean ± s.e.m, −0.013 ± 0.005, $p = 0.019$). More specifically, compared to baseline, the mean similarity index significantly reduced when the dopamine concentration reached 300–1000 μM (mean ± s.e.m of % change in the mean similarity index: 0 ± 8%, −11 ± 10%, −24 ± 7%, −30 ± 12% for 30, 100, 300, 1000 μM DA conditions, respectively, as depicted in Fig. 5B). It's noteworthy that this reduction in similarity remained consistent irrespective of the size of the temporal window (Supplementary Fig S3C).

Compared to the baseline, the number of repeating motifs increased by approximately 40–50% when the dopamine concentration reached 300–1000 μM. However, this increase was not statistically significant (linear mixed-effects model with the number of repeating motifs as the response variable: mean ± s.e.m of DA coefficient, 0.1 ± 0.2, $p = 0.6$, Fig. 5C). In contrast, higher dopamine concentrations significantly increased the motif size, which refers to the number of bursts in repeating motifs. This was demonstrated by a linear mixed-effects model with motif size as the response variable (mean ± s.e.m of DA coefficient, 6.3 ± 2.5, $p = 0.016$). The mean ± s.e.m percentage change in motif size relative to the baseline level was 19 ± 17%, 68 ± 51%, 42 ± 12%, and 50 ± 17% for 30, 100, 300, and 1000 μM DA conditions, respectively (Fig. 5D).

One may ask whether the divergence of burst patterns was indeed influenced by elevated dopamine concentrations rather than an increase

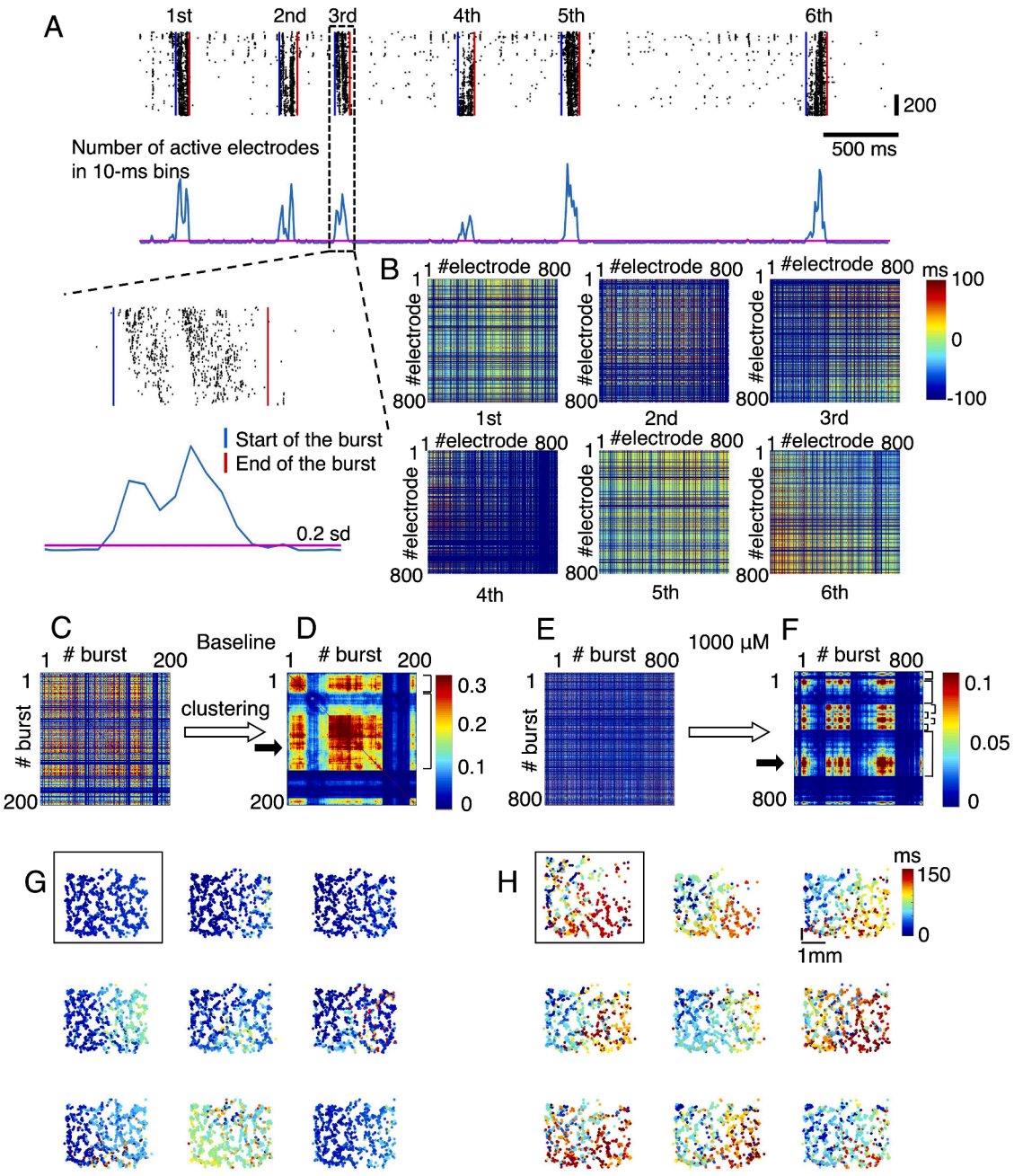

Fig. 4. Analysis of Synchronized Bursting Events in a Representative Sample.
A: Synchronised bursting events were identified based on timings when the number of active electrodes in 10-msec bins exceeded and fell below the threshold (magenta line), respectively. B: For each of the detected bursts, the activation pattern was constructed by capturing the differences in timing of the first spike in the burst between all electrode pairs. The six color maps depict activation patterns of the bursts detected in Fig. 4A. C-D: A similarity matrix was constructed for all pairs of bursting events in the baseline condition of the representative sample (C). Using affinity propagation, we detected two repeating motifs of bursting patterns, which are marked by the parentheses on the right side of the sorted similarity matrix (D). E-F: similar to C-D but for the condition of 1000 μM DA level. There were 7 repeating motifs detected in this data condition. G: Scatter plots showing the relative position of the electrodes, with the color, scaled from 0 to 150 msec, illustrating the delay of the first spike timing of each electrode to the start of the burst. The scatter plot shown in the box was for a reference burst (indicated by solid black arrow in D), and the remaining 8 scatter plots represent the 8 bursts with the highest similarity to the reference burst. H: Similar to G but for the condition of 1000 μM DA level.

in the number of bursts (Fig. 5A). To answer this question, for each sample, we randomly selected an equivalent number of bursts ($n = 100$ or fewer if fewer bursts were present) in both the baseline and 1000 μM DA condition. We then computed the mean similarity index between the sampled bursts within the same condition. This resampling procedure was repeated 1000 times. As a result, six out of eight samples exhibited a significantly smaller mean similarity index in the 1000 μM DA condition compared to the baseline (Fig. 5E). While the remaining two samples showed a slight increase in the mean similarity index in the 1000 μM DA condition, this trend was also evident in the original similarity index distribution (Supplementary Fig S6).

Dopamine-induced decrease in synchrony strength causally decreases the similarity of activation patterns

In our final exploration, we investigated the causal relationship between the decrease in network synchrony and the resulting increase in burst pattern diversity through pharmacological intervention.

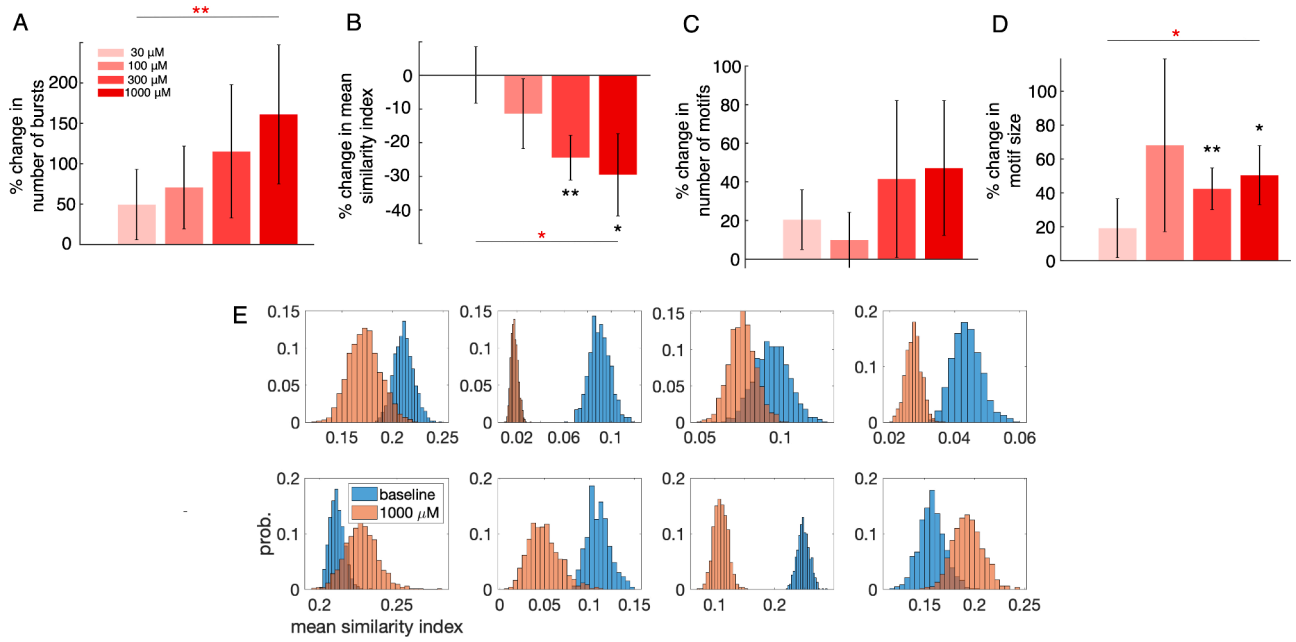

Fig. 5. Dopamine diversifies activation patterns in burst events.
A-D: Number of bursts (A), the mean similarity index between bursts (B), number of repeating motifs (C), and the motif size (D), normalized by the baseline level, for the four DA conditions, $n = 8$ samples. Bars with errors represent mean and s.e.m, respectively. The convention was the same as in Fig 2. E: Probability distributions of the mean similarity index for the 8 samples following 1000 random resampling of the equivalent number of bursts in the baseline (blue bars) and 1000 μM DA condition (orange bars).

Specifically, we tested the D2-receptor antagonist sulpiride and the D1-receptor antagonist SCH23390 (see Methods). We observed a notable effect of dopamine on synchrony strength (linear mixed-effects model, mean ± s.e.m of DA coefficient, -0.0012 ± 0.0003, $p < 0.001$) but not the similarity index ($p = 0.08$) in $n = 12$ samples treated with the D2-receptor antagonist sulpiride. Among the $n = 9$ samples administered with the D1-receptor antagonist SCH23390, there were no significant dopamine effects identified ($p > 0.2$). Importantly, through an examination of inter-sample variability, we found a significant and positive relationship between the change in synchrony strength induced by dopamine and the change in similarity index across samples with no antagonist (linear regression, $R^2 = 0.22$, $p = 0.02$, represented by red circles in Fig. 6). Notably, this correlation was absent in samples treated with either SCH23390 ($R^2 = 0.04$, $p = 0.33$, purple triangles) or sulpiride ($R^2 = 0.06$, $p = 0.19$, grey squares). These findings suggest that the dopamine-induced decrease in synchrony strength within hippocampal networks directly contributes to the divergence in their activation patterns.

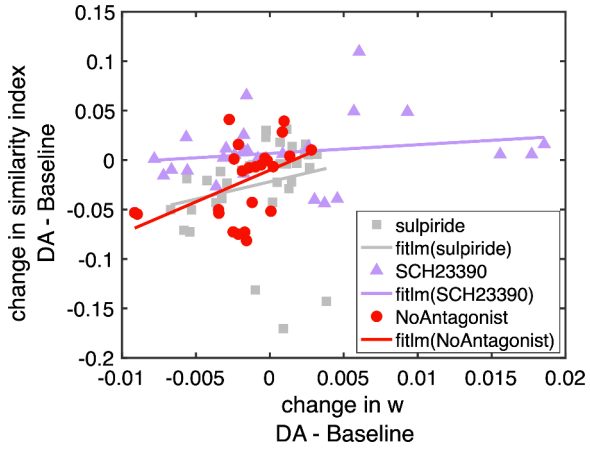

Fig. 6. Correlation of synchrony strength and similarity in activation patterns.
The changes in similarity index (ordinate) were plotted against the changes in averaged synchrony strength (abscissa), and regression analysis was performed for three groups: samples with no dopamine antagonist ($n = 32$, red circles), samples with sulpiride ($n = 48$, grey squares), and samples with SCH23390 ($n = 35$, purple triangles). Note that each sample has 4 DA concentration conditions in comparison with their baseline condition.

Discussion

In this study, we examined the spiking activity of cultured hippocampal neurons under the influence of dopamine. By gradually administering dopamine, we observed a significant increase in the number of burst events, characterised by highly synchronised spikes across hundreds of electrodes within a 200–300 ms timeframe (Fig. 1), consistent with previous findings (Li et al., 2017; Miyawaki et al., 2014). The high density of electrodes in our setup allowed us to monitor hippocampal neuron activity with cellular spatial and millisecond temporal resolution, enabling us to examine the effects of dopamine from a network-level perspective. Our observations revealed that dopamine administration resulted in a decrease in spike synchrony within cultured hippocampal networks (Fig. 2). Additionally, dopamine increased the number of network modules, where each exhibited more confined connectivity (Fig. 3). These findings imply that dopamine serves to restructure hippocampal networks, potentially influencing the flow of information in cognitive processes such as memory formation, decision-making, and attentional control (Lisman & Grace, 2005; Floresco & Grace, 2003; Schultz, 2007; Takahashi et al., 2008; Lemon et al. 2009; Smith & Greene, 2012). Supporting this hypothesis, our study also revealed that dopamine reduced the similarity in activation patterns between bursts and increased the number of repeating motifs (Figs. 4 and 5). This expansion in the repertoire of burst dynamics may lead to a more distinct and separable encoding of information within the hippocampal circuitry (Sporns & Kötter, 2004; Chadwick & Hassabis, 2017; Ritchey et al., 2013; Staresina & Davachi, 2008). Interestingly, the diversification of firing patterns induced by dopamine was similarly reported by Miyawaki et al. (2014). Their study demonstrated that upon activation of dopamine receptors, different subsets of neurons were co-activated in sharp-wave events. This phenomenon was observed at a

much higher spatio-temporal resolution in our study (Fig. 4G–H). Most notably, we demonstrated that dopamine-induced decreases in synchrony correlate with reductions in the similarity index, a correlation absent in samples treated with either D1 or D2-receptor antagonist (Fig. 6). An intriguing observation arises when considering that sulpiride, a medication used to treat schizophrenia, may potentially maintain the inherent structure of hippocampal networks while inhibiting the diversification of brain activity, a characteristic feature often observed in individuals with schizophrenia (Shiloh et al. 1997). Future studies of dopamine-mediated signaling using knock-in rats may provide valuable insights into the pathology of this disorder (Matsumoto et al., 2024).

It is important to differentiate spike synchrony from functional connectivity (e.g., synaptic connectivity) between nodes (Cai et al., 2017; Kobayashi et al., 2019; Vareberg et al., 2024). This distinction is necessary because inferring functional connectivity from spike trains requires a relatively large number of spikes (Kobayashi et al., 2019), which is not feasible with our data. Our recordings have a mean firing rate of approximately 2 Hz over about 300 s per condition, resulting in an average of only 600 spikes per electrode. Consequently, this study focuses on the effects of dopamine on synchrony strength in the hippocampal network rather than on functional connectivity. It is also noteworthy that the dopamine concentration levels of 30–1000 μM examined in this study are much higher than those measured in an intact brain Zetterström et al. (1983); Sharp et al. (1986); Borgkvist et al. (2012). However, similar DA concentrations have been reported as necessary to yield observable effects in the in vitro hippocampal neurons (Behr et al., 2000; Weiss et al., 2003; Wang et al., 2020), a phenomenon also present in our investigation of firing rates (Supplementary Fig S1). Regarding the firing activity, hippocampal cultures typically display short-duration bursts, with significantly longer interburst intervals (as illustrated in Fig. 1B). Suresh et al. (2016) highlighted the crucial role of intrinsic membrane dynamics in burst initiation during interburst intervals, while synaptic processes operating on shorter timescales influence properties within-bursts and network synchrony. In our observations, the influence of dopamine on interburst activity remains uncertain, despite showing a modest increase in firing rate (linear mixed-effects models with firing rate in interburst intervals as response variable, $p = 0.048$). This suggests that dopamine may have a more profound impact on synaptic processes than on membrane dynamics. Nonetheless, further simulation work is required to dissect the specific effects of dopamine on spiking patterns at different timescales.

In summary, our study offers new insights into the causal relationship between dopamine-induced decreases in spike synchrony and the expansion of firing pattern repertoire within hippocampal networks. By elucidating the mechanisms underlying dopamine-mediated modulation of information processing, we contribute to a deeper understanding of the neural basis of hippocampus-dependent cognitive processes.

Methods

Ethical approval

Animal experiments were performed with the approval of the Animal Experiment Ethics Committee at the University of Tokyo (approval numbers: P29–3, P4–12) and according to the University of Tokyo guidelines for the care and use of laboratory animals. These experimental protocols were carried out in accordance with the Fundamental Guidelines for the Proper Conduct of Animal Experiments and Related Activities in Academic Research Institutions (Ministry of Education, Culture, Sports, Science and Technology, Notice No 71 of 2006), the Standards for Breeding and Housing of and Pain Alleviation for Experimental Animals (Ministry of the Environment, Notice No 88 of 2006) and the Guidelines on the Method of Animal Disposal (Prime Minister's Office, Notice No 40 of 1995). All efforts were made to minimize animal suffering.

Animals

Embryonic day (E) 18 pregnant female Wistar/ST rats (Japan SLC, Shizuoka, Japan) were housed in a controlled environment with regulated temperature and humidity (22 ± 1 °C, 55 ± 5%) and maintained on a 12:12-hour light/dark cycle. Access to food and water was provided ad libitum throughout the duration of the study.

Preparation

MaxOne high-density multi-electrode array (HD-MEA) chips (Maxwell Biosystems, Zurich, Switzerland) were pretreated and coated according to the manufacturer's protocol. Briefly, 1% w/v Terg-a-zyme (Z273287, Merck, Darmstadt, Germany), dissolved in ultrapure water, was placed on each chip overnight for hydrophilization. On the next day, the Terg-a-zyme solution was removed. The chips and their lids were rinsed with ultrapure water three times and immersed in 70% ethanol for 30 min for sterilization. After rinsing with ultrapure water and drying them, a coating solution was prepared, which was composed of 50% poly(ethyleneimine) (PEI) solution (P3143, Merck), 20× borate buffer (28,341, Thermo Fisher Scientific, MA, USA), and ultrapure water at a final ratio of 140:4993:94,867. The coating solution was sterilized by filtering and directly added to the HD-MEA. The chip was covered with its lid, incubated in 5% CO_2 at 37 °C for 1 h, washed with ultra-pure water three times, and dried in air.

Primary cultures of hippocampal neurons were prepared from hippocampi of embryos of either sex as follows. The E18 rat was deeply anaesthetized by inhalation of an overdose of isoflurane, followed by intraperitoneal injection of a cocktail of xylazine (in saline, 12 mg/kg) and pentobarbital (in saline, 40 mg/kg). The rat's uterus was carefully extracted and immersed in sterilized Ca^{2+}- and Mg^{2+}-free Hanks' balanced salt solution (HBSS(-)) on ice, after which the mother rat was euthanized. The embryonic brains were extracted under microscopy and immersed in HBSS(-). The hippocampi were then dissected out. For the next step, Geltrex (A1569601, Thermo Fisher Scientific) was added to the coated HD-MEA chip, after which it was incubated in 5% CO_2 at 37 °C for 1 h.

After dissection, the hippocampi were minced using a surgical knife, collected in additional HBSS(-), treated with 0.05% Trypsin-EDTA (25,300,062, Thermo Fisher Scientific), and incubated at 37 °C for 15 min, followed by further incubation with 1% DNase I (in saline) (10,104,159,001, Merck) at room temperature for 5 min and removal of the supernatant. Tissues were washed in HBSS(-) and incubated (in a bath) at 37 °C for 5 min, after which the supernatant was removed. This procedure was repeated three times. Tissues were then triturated using a fire-polished Pasteur pipette in Neurobasal medium (12,349,015, Thermo Fisher Scientific) containing 2% B27 supplement (17,504,044, Thermo Fisher Scientific), 0.5 mM glutamine, 25 μM glutamate, 1 mM 4-(2-hydroxyethyl)−1-piperazineethanesulfonic acid (HEPES), 0.5% penicillin-streptomycin (09,367–34, Nacalai Tesque, Kyoto, Japan), and 10% horse serum (26,050,088, Thermo Fisher Scientific), which we called plating medium. The tissues were further filtered through 100-μm-pore cell strainers, and centrifuged at 700 × g at 25 °C for 5 min. The supernatant was replaced with a plating medium, which produced suspension. The suspension was mixed with nigrosin (198,285, Merck) at a ratio of 1:1 to count the cells and calculate cell density on a hemocytometer (erythrocytometer). The initial cell concentration on Day 0 in vitro (DIV 0) was adjusted to 6×10^3 cells/μl unless otherwise specified; the initial cell density was ~6×10^3 cells/mm^2 because the whole area on the chip and cell drop volume were ~50 mm^2 and 50 μl, respectively. Cells were dispersed and seeded on the HD-MEA and incubated in 5% CO_2 at 37 °C for 1 h under maintained humidity, after which the plating medium was added to the MEA.

The feeding medium consisted of 2% B27, 1 mM HEPES, 0.5 mM glutamate, and 0.5% penicillin-streptomycin in Neurobasal medium and was used when the medium was replaced except for DIV 2. On DIV 1, the

full medium was replaced with the feeding medium. On DIV 2, the full medium was replaced with the feeding medium including 5 μM cytosine arabinoside (AraC) to suppress the non-neuronal cell proliferation. On DIV 3, the full medium was refreshed. Afterwards, half of the medium was replaced twice a week. Every time the medium was replaced, the condition of the cultured neurons was checked with the eye to confirm that there was no evidence that active neurons were obviously contaminated, damaged, or dying.

In vitro electrophysiology

The MaxOne recording system (Maxwell Biosystems) including the CMOS-based HD-MEA and MaxLab Live software (Maxwell Biosystems) including predefined pipelines were used to record and visualize the extracellular action potentials of the cultured hippocampal neurons. The HD-MEA chip had 26,400 platinum electrodes, organized in 220 × 120 pixels. The active sensing area was 3.85 × 2.10 mm^2. The centre-to-centre electrode distance was 17.5 μm. Neural activity was measured at a sampling frequency of 20 kHz simultaneously from up to 1024 channels in experimenter-based configurations with 10-bit analog-to-digital converter resolution.

The recording system was situated inside a 5% CO2 incubator at 37 °C. Spontaneous neuronal activity was recorded from all channels using the 'Activity scan' module for 10 min, extracting the most 'active' 1024 channels based on the firing rate. Identification of active channels subsequently allowed us to monitor collective neuronal activity using the 'Network' module for 5 min. The 'Network' recording was performed as follows. First, (1) dopamine (50 μM, 1 μl) was added to the chip (containing 500 μl medium) to achieve a final concentration of 0.1 μM dopamine. Neural activity was recorded at 0.1 μM dopamine using the 'Network' module. Next, dopamine was added in varying amounts ((2) 50 μM, 2 μl; (3) 50 μM, 7 μl; (4) 500 μM, 2 μl; (5) 500 μM, 7 μl; (6) 5 mM, 2 μl; (7) 5 mM, 7 μl; (8) 50 mM, 2 μl; (9) 50 mM, 7 μl; (10) 500 mM, 2 μl; (11) 500 mM, 7 μl; (12) 1 M, 10 μl) and neural activity was recorded at the following concentrations: (2) 0.3 μM; (3) 1 μM; (4) 3 μM; (5) 10 μM; (6) 30 μM; (7) 100 μM; (8) 300 μM; (9) 1 mM; (10) 3 mM; (11) 10 mM; (12) 30 mM. We systematically examined the firing rate of the samples at all recorded concentration levels and found that concentrations ranging from 30 μM to 1 mM consistently elevated the firing rate compared to baseline (Supplementary Fig S1). When the concentration level exceeded 1 mM (i.e., conditions (10)-(12)), the electrodes became completely silent (data not shown). Therefore, we focused on analyzing the effects of dopamine within the 30 μM to 1 mM concentration range. In antagonist experiments, sulpiride (25 mM, 2 μL) or SCH23390 (2.5 mM, 2 μL) was added to the chip to achieve a final concentration of 100 μM or 10 μM, respectively, before recording session (1). Recordings were regularly performed once a week.

Preprocessing of in vitro spike trains

A considerable number of electrodes had relatively low activity during recordings. To address this issue, we implemented the following procedure for electrode selection. Initially, we assessed the number of active electrodes in time bins of 10 msec using all available electrodes. Subsequently, we systematically identified the top 90% of active electrodes based on their firing rates and determined the number of active electrodes using this subset. We then computed the correlation in the number of active electrodes between the two conditions. This process was repeated for subsets ranging from the top 80% to the top 10% of active electrodes. We found that the correlation remained consistently high (>0.99), even when considering only the top 50% of active electrodes (refer to Supplementary Fig S2). Based on these findings, we established that the correlation remained robust irrespective of the proportion of active electrodes considered. Consequently, in our analyses of all the samples, we opted to use the top 80% of active electrodes while discarding the remaining 20% of electrodes. We note that, after preprocessing, 95 ± 2% of the electrodes selected were consistent between baseline and DA conditions. This approach ensured a standardized and representative selection of electrodes for our analyses, enhancing the reliability and consistency of our results.

Network analysis

In our study, networks were represented by synchrony matrices, where rows and columns corresponded to electrodes. The entries in these matrices indicated synchrony strength, determined by the number of spikes co-activated within 1 msec bins:

$$w_{i,j} = \frac{1}{\sqrt{N_i \times N_j}} \sum_{t=1:T} s_i(t) \times s_j(t)$$

Here, $s_i(t)$ represents the number of spikes from the i th electrode in the t-th bin, and N_i represents the total number of spikes from the i th electrode over the entire recording time T.

The modularization of the network involved dividing it into non-overlapping groups of electrodes, aiming to maximise the number of within-group weights while minimising the number of between-group weights. To detect these modules, we used the Brain Connectivity Toolbox (Rubinov & Sporns, 2010), employing the method of optimal modularity (Newman, 2006). If a module consists of only one electrode, it is reassigned to the nearest module based on its position.

Additionally, we computed the participation coefficient for each electrode. This coefficient measures the strength of a node's connections within its module (Guimerà & Nunes Amaral 2005). The distance between nodes was defined by the Euclidean distance of the relative positions of the electrodes on the MaxOne chip.

Detection of bursting events and evaluation of activation patterns in bursts

To detect bursting events, spikes were first binned into 10-msec intervals. The onset and offset of each burst were then identified by determining timings when the number of active electrodes exceeded and subsequently fell below a predefined threshold. This threshold was consistently set at 0.2 standard deviations. Bursts lasting <50 msec were excluded.

We adopted a similar approach to Raichman and Ben-Jacob (2008) to quantitatively assess the activation patterns across bursts. For each burst, the activation pattern was characterised by a matrix A_k, where $A_k(i,j)$ represents the delay in milliseconds between the first spike of the i-th electrode $\bar{s}_i^k$ and the first spike of the j-th electrode $\bar{s}_j^k$ in the k-th burst:

$$A_k(i,j) = \bar{s}_i^k - \bar{s}_j^k$$

If an electrode did not fire during a particular burst, its value was set as NULL.

The similarity index $S(A_p, A_q)$ between burst p and q was computed as follows:

$$S(A_p, A_q) = \frac{1}{n(n-1)} \sum_{i \neq j} H\left(th - \left|A_p(i,j) - A_q(i,j)\right|\right)$$

Where n denotes the number of electrodes, H is the Heaviside step function, defined as $H(x) = 0$ if $x < 0$ and $H(x) = 1$ if $x \geq 0$, and th is a time-threshold parameter. In this equation, $S(A_p, A_q)$ represents the fraction of neuron pairs (i,j) for which the difference in delays between the two bursts is less than th: $|A_p(i,j) - A_q(i,j)| < th$. The summation is conducted only over neuron pairs (i,j) that did not receive NULL values in either burst (i.e., both neurons fired a spike in both bursts). In our analysis, we set $th = 50$ msec to reflect the average spike precision in bursts. We also tested other values of th ranging from 10 to 100 msec, and the results remained consistent (Supplementary Fig S2).

Detection of repeating motifs from the similarity matrix by affinity propagation

We applied the affinity propagation algorithm (Frey & Dueck, 2007) on the similarity matrix to identify clusters of burst patterns. Affinity propagation identifies exemplar points within the dataset and forms clusters around these exemplars. In our analysis, the algorithm used the similarities between pairs of burst patterns (described above) to automatically determine the optimal number of clusters based on the preference parameter $p(i)$, which indicates the preference that the i-th data point is chosen as a cluster exemplar. We set all preference values to the median of the similarity matrix.

Following affinity propagation clustering, a cluster is considered as a repeating motif if it met two criteria: size and separation.

1. *Size*: The number of bursts in a cluster must exceed $\sqrt{N_b}$, where N_b represents the total number of bursts. This threshold offers two key advantages. First, it reliably captures the repetitive nature of the repeating motif (Raichman & Ben-Jacob, 2008). Second, it serves as a normalization factor to account for differences in the total number of bursts across various data conditions.
2. *Separation*: A cluster is considered well separated from other clusters if the mean similarity score between bursts within the same cluster (within-cluster) is statistically greater than the mean similarity score between bursts in that cluster and all other bursts (across-cluster). This comparison is conducted using a two-sample t-test with a significance threshold of $p < 0.01$. We note that, due to the curse of dimensionality, where the burst pattern is highly dimensional ($n \times n$, with n representing the number of electrodes), clusters often exhibit high similarity, and the number of bursts is limited. As a result, traditional clustering validation metrics like the silhouette score may perform poorly. Therefore, statistical tests offer a more reliable method for validating the separation and quality of the clusters (Supplementary Figure S4A).

We observed that although the number of clusters increased with an increase in the preference parameter, the detected repeating motifs remained stable (Supplementary Figure S4B). The affinity propagation algorithm also outperformed traditional clustering methods, such as hierarchical clustering, when faced with high data complexity (Supplementary Figure S4C). Additionally, we systematically explored the robustness of affinity propagation by varying the preference parameter from 20% to 150% of the median similarity index. Our results showed that the dopamine-induced change in the number of repeating motifs remained unchanged across this range of the preference parameter (Supplementary Figure S4D).

Statistical analysis

We used linear mixed-effect models to statistically evaluate the influence of dopamine on the metrics of interest, such as synchrony strength and similarity index. Each model was structured as $Metric \sim Concentration\ Level + (1 \mid Sample)$, where *Metric* is the metric of interest, *Concentration Level* represents the 10-base logarithm of dopamine concentration in the bath (with a value of 0 for the baseline condition), and $(1 \mid Sample)$ accounts for repeated measures within each sample, thus adding a random effect for the intercept. Note that the logarithm represents the quantity of dopamine added during the experiments and does not alter the observed trend in the data. This analysis was conducted using the MATLAB function *fitlme*, from which we obtained the coefficient of *Concentration Level* and its corresponding significance p-value. Additionally, to assess the significance of dopamine-induced changes in these metrics relative to the baseline, we applied the following normalization: $(Metric_{DA} - Metric_{Baseline}) / Metric_{Baseline}$, where $Metric_{Baseline}$ denotes the corresponding metric in the absence of dopamine. Subsequently, one-tailed t-tests were employed to determine whether the distributions of the metrics were significantly different from zero, representing the baseline level.

To evaluate inter-sample variability depicted in Fig. 6, we employed a linear model to analyse the relationship between the amount of changes in synchrony strength and the amount of changes in the similarity index across samples. This analysis was conducted using the MATLAB function *fitlm*, from which we obtained the coefficient of determination (R^2) and significance p-value. Throughout the paper, the significance levels were determined as follows: n.s (not significant) for $p > 0.05$, * for $p < 0.05$, ** for $p < 0.01$. These significance levels were used to interpret the statistical significance of the observed relationships. Unless specifically stated elsewhere, the mean ± *s*.e.m of the statistics across samples were reported.

CRediT authorship contribution statement

Huu Hoang: Writing – review & editing, Writing – original draft, Visualization, Software, Methodology, Investigation, Formal analysis. **Nobuyoshi Matsumoto:** Writing – review & editing, Writing – original draft, Validation, Resources, Investigation, Data curation. **Miyuki Miyano:** Writing – review & editing, Writing – original draft, Resources, Investigation, Data curation. **Yuji Ikegaya:** Writing – review & editing, Writing – original draft, Supervision, Project administration, Funding acquisition, Conceptualization. **Aurelio Cortese:** Writing – review & editing, Writing – original draft, Supervision, Methodology, Investigation, Formal analysis, Conceptualization.

Declaration of competing interest

The authors declare that they have no known competing financial interests or personal relationships that could have appeared to influence the work reported in this paper.

Acknowledgements

This study was supported by JST ERATO (JPMJER1801, "Brain-AI hybrid"). HH and AC were additionally supported by Grants-in-Aid for Transformative Research Areas (22H05160). HH were partially supported by Grant Number JP23dm0307002, Japan Agency for Medical Research and Development (AMED).

Supplementary materials

Supplementary material associated with this article can be found, in the online version, at doi:10.1016/j.neunet.2024.106888.

Data availability

The customized MATLAB code of the analyses and spiking data of the samples was hosted publicly on github, accessible via https://github.com/hoang-atr/MaxOne.

References

Behr, J., Gloveli, T., Schmitz, D., & Heinemann, U. (2000). Dopamine depresses excitatory synaptic transmission onto rat subicular neurons via presynaptic D1-like dopamine receptors. *The Journal of Neurophysiology, 84*(1), 112–119.

Borgkvist, A., Malmlöf, T., Feltmann, K., Lindskog, M., & Schilström, B. (2012). Dopamine in the hippocampus is cleared by the norepinephrine transporter. *The International Journal of Neuropsychopharmacology, 15*(4), 531–540.

Bullmore, E., & Sporns, O. (2009). Complex brain networks: Graph theoretical analysis of structural and functional systems. *Nat Rev Neurosci, 10*(3), 186–198.

Cai, Z., Neveu, C. L., Baxter, D. A., Byrne, J. H., & Aazhang, B. (2017). Inferring neuronal network functional connectivity with directed information. *The Journal of Neurophysiology, 118*, 1055–1069.

Chadwick, M. J., & Hassabis, D. (2017). Hippocampal substrates of sensory and mnemonic representations in the human brain. *The Proceedings of the National Academy of Sciences, 114*(40), 10218–10223.

da Silva, W. C., Köhler, C. C., Radiske, A., & Cammarota, M. (2012). D1/D5 dopamine receptors modulate spatial memory formation. *The Neurobiology of Learning and Memory, 97*, 271–275.
Floresco, S. B., & Grace, A. A. (2003). Gating of hippocampal-evoked activity in prefrontal cortical neurons by inputs from the mediodorsal thalamus and ventral tegmental area. *The Journal of Neurophysiology, 23*(9), 3930–3943.
Frey, B. J., & Dueck, D. (2007). Clustering by passing messages between data points. *Science (New York, N.Y.), 315*(5814), 972–976.
Friston, K. (2011). Functional and effective connectivity: A review. *Brain Connectivity, 1*(1), 13–36.
Gasbarri, A., Sulli, A., & Packard, M. G. (1997). The dopaminergic mesencephalic projections to the hippocampal formation in the rat. *Prog Neuropsychopharmacol Biol Psychiatry, 21*(1), 1–22.
Gonzalez-Sulser, A., Wang, J., Queenan, B. N., Avoli, M., Vicini, S., & Dzakpasu, R. (2012). Hippocampal neuron firing and local field potentials in the in vitro 4-aminopyridine epilepsy model. *The Journal of Neurophysiology, 108*(9), 2568–2580.
Grace, A. A. (2012). Dopamine system dysregulation by the hippocampus: Implications for the pathophysiology and treatment of schizophrenia. *Neuropharmacology, 62*(3), 1342–1348.
Grace, A. A. (2016). Dysregulation of the dopamine system in the pathophysiology of schizophrenia and depression. *Nature Reviews Neuroscience, 17*(8), 524–532.
Guimerà, R., & Nunes Amaral, L. A (2005). Functional cartography of complex metabolic networks. *Nature, 433*(7028), 895–900.
Kayama, T., Suzuki, I., Odawara, A., Sasaki, T., & Ikegaya, Y. (2018). Temporally coordinated spiking activity of human induced pluripotent stem cell-derived neurons co-cultured with astrocytes. *Biochem. Biophys. Res. Commun, 495*, 1028–1033.
Kempadoo, K. A., Mosharov, E. V., Choi, S. J., Sulzer, D., & Kandel, E. R. (2016). Dopamine release from the locus coeruleus to the dorsal hippocampus promotes spatial learning and memory. *Proceedings of the National Academy of Sciences of the United States of America., 113*(51), 14835–14840.
Kobayashi, R., Kurita, S., Kurth, A., et al. (2019). Reconstructing neuronal circuitry from parallel spike trains. *Nature Communications, 10*, 4468.
Lemon, N., Aydin-Abidin, S., Funke, K., & Manahan-Vaughan, D. (2009). Locus coeruleus activation facilitates memory encoding and induces hippocampal LTD that depends on β-adrenergic receptor activation. *Cereb Cortex, 19*(12), 2827–2837.
Li, Y., Chen, X., Dzakpasu, R., & Conant, K. (2017). Dopamine-dependent effects on basal and glutamate stimulated network dynamics in cultured hippocampal neurons. *The Journal of Neurophysiology, 140*(4), 550–560.
Lisman, J. E. (2011). Dopamine and the salience of time. *The Journal of Neuroscience, 31*(26), 9567–9568.
Lisman, J., Grace, A. A., & Duzel, E. (2011). A neoHebbian framework for episodic memory; role of dopamine-dependent late LTP. *Trends Neurosci, 34*(10), 536–547.
Lisman, J. E., & Grace, A. A. (2005). The hippocampal-VTA loop: Controlling the entry of information into long-term memory. *Neuron, 46*(5), 703–713.
Matsumoto, N., Miyano, M., Abe, T., Kashima, T., Kato-Ishikura, E., Inoue, K., Liu, J., Kiyonari, H., Takeuchi, H., & Ikegaya, Y. (2024). Generation of dopamine transporter (DAT)-mCherry knock-in rats by CRISPR-Cas9 genome editing. *Biological and Pharmaceutical Bulletin, 47*, 394–398.
McNamara, C. G., Tejero-Cantero, Á., Trouche, S., Campo-Urriza, N., & Dupret, D. (2014). Dopaminergic neurons promote hippocampal reactivation and spatial memory persistence. *Nature Neuroscience, 17*(12), 1658–1660.
McNamara, C. G., & Dupret, D. (2017). Two sources of dopamine for the hippocampus. *Trends Neurosci, 40*(7), 383–384.
Miyawaki, T., Norimoto, H., Ishikawa, T., Watanabe, Y., Matsuki, N., & Ikegaya, Y. (2014). Dopamine Receptor Activation Reorganizes Neuronal Ensembles during Hippocampal Sharp Waves In Vitro. *PLoS One, 9*(8), Article E104438.
Mody, I., & Staley, K. J. (1994). Cell properties in the epileptic hippocampus. *Hippocampus, 4*(3), 275–280.
Newman, M. E. (2006 Jun 6). Modularity and community structure in networks. *Proc Natl Acad Sci USA., 103*(23), 8577–8582.
Niedringhaus, M., Chen, X., Conant, K., & Dzakpasu, R. (2013). Synaptic potentiation facilitates memory-like attractor dynamics in cultured in vitro hippocampal networks. *PLoS One, 8*(3), E57144.
Pimashkin, A., Kastalskiy, I., Simonov, A., Koryagina, E., Mukhina, I., & Kazantsev, V. (2011). Spiking signatures of spontaneous activity bursts in hippocampal cultures. *Frontiers in Computational Neuroscience, 5*, 46.
Raichman, N., & Ben-Jacob, E. (2008). Identifying repeating motifs in the activation of synchronized bursts in cultured neuronal networks. *Journal of Neuroscience Methods, 170*(1), 96–110.
Ritchey, M., Wing, E. A., LaBar, K. S., & Cabeza, R. (2013). Neural similarity between encoding and retrieval is related to memory via hippocampal interactions. *Cereb Cortex, 23*(12), 2818–2828.
Rubinov, M., & Sporns, O. (2010 Sep). Complex network measures of brain connectivity: Uses and interpretations. *Neuroimage, 52*(3), 1059–1069.
Sasaki, T., Suzuki, I., Yokoi, R., Sato, K., & Ikegaya, Y. (2019). Synchronous spike patterns in differently mixed cultures of human iPSC-derived glutamatergic and GABAergic neurons. *Biochemical and Biophysical Research Communications., 513*, 300–305.
Schultz, W. (2007). Multiple dopamine functions at different time courses. *Annual Review of Neuroscience, 30*(1), 259–288.
Sharp, T., Zetterström, T., & Ungerstedt, U. (1986). An in vivo study of dopamine release and metabolism in rat brain regions using intracerebral dialysis. *The Journal of Neuroscience, 47*(1), 113–122.
Shiloh, R., Zemishlany, Z., Aizenberg, D., et al. (1997). Sulpiride augmentation in people with schizophrenia partially responsive to clozapine: A double-blind, placebo-controlled study. *British Journal of Psychiatry, 171*(6), 569–573.
Shohamy, D., & Adcock, R. A. (2010). Dopamine and adaptive memory. *Trends in Cognitive Sciences, 14*(10), 464–472.
Smith, C. C., & Greene, R. W. (2012). CNS dopamine transmission mediated by noradrenergic innervation. *The Journal of Neuroscience, 32*(18), 6072–6080.
Sporns, O., & Kötter, R. (2004). Motifs in brain networks. *PLoS Biol, 2*(11), E369.
Staresina, B. P., & Davachi, L. (2008). Selective and shared contributions of the hippocampus and perirhinal cortex to episodic item and associative encoding. *Journal of Cognitive Neuroscience, 20*(8), 1478–1489.
Suresh, J., Radojicic, M., Pesce, L. L., Bhansali, A., Wang, J., Tryba, A. K., Marks, JD, & van Drongelen, W. (2016). Network burst activity in hippocampal neuronal cultures: The role of synaptic and intrinsic currents. *The Journal of Neuroscience, 115*(6), 3073–3089.
Swanson, L. W. (1982). The projections of the ventral tegmental area and adjacent regions: A combined fluorescent retrograde tracer and immunofluorescence study in the rat. *Brain Research Bulletin, 9*(1–6), 321–353.
Takahashi, H., Kato, M., Takano, H., Arakawa, R., Okumura, M., Otsuka, T., & Suzuki, K. (2008). Differential contributions of prefrontal and hippocampal dopamine D(1) and D(2) receptors in human cognitive functions. *The Journal of Neuroscience, 28*(46), 12032–12038.
Takeuchi, T., Duszkiewicz, A. J., Sonneborn, A., Spooner, P. A., Yamasaki, M., Watanabe, M., Smith, CC, Fernández, G, Deisseroth, K, Greene, RW, & Morris, RG. (2016). Locus coeruleus and dopaminergic consolidation of everyday memory. *Nature, 537*(7620), 357–362.
Vareberg, A. D., Bok, I., Eizadi, J., Ren, X., & Hai, A (2024). Inference of network connectivity from temporally binned spike trains. *The Journal of Neuroscience Methods, 404*, Article 110073.
Wang, L., Zhao, D., Wang, M., Wang, Y., Vreugdenhil, M., Lin, J., & Lu, C (2020). Modulation of Hippocampal Gamma Oscillations by Dopamine in Heterozygous Reeler Mice in vitro. *Frontiers in Cellular Neuroscience, 13*, 586.
Weiss, T., Veh, R. W., & Heinemann, U. (2003). Dopamine depresses cholinergic oscillatory network activity in rat hippocampus. *The European Journal of Neuroscience, 18*(9), 2573–2580.
Wise, R. A. (2004). Dopamine, learning and motivation. *Nature Reviews Neuroscience, 5*(6), 483–494.
Xie, X., Li, M., Feng, B., Li, J., Sun, Z., Zhao, Y., & Lu, C. (2011). The Cellular Mechanisms of Dopamine Modulation on the Neuronal Network Oscillations in the CA3 Area of Rat Hippocampal Slices. *Neuroscience, 475*, 83–92.
Xing, B., Kong, H., Meng, X., Wei, S. G., Xu, M., & Li, S. B. (2010). Dopamine D1 but not D3 receptor is critical for spatial learning and related signaling in the hippocampus. *Neuroscience, 169*(4), 1511–1519.
Yamada, M. K., Nakanishi, K., Ohba, S., Nakamura, T., Ikegaya, Y., Nishiyama, N., & Matsuki, N. (2002). Brain-derived neurotrophic factor promotes the maturation of GABAergic mechanisms in cultured hippocampal neurons. *The Journal of Neuroscience : The Official Journal of the Society for Neuroscience, 22*, 7580–7585.
Zetterström, T., Sharp, T., Marsden, C. A., & Ungerstedt, U. (1983). In vivo measurement of dopamine and its metabolites by intracerebral dialysis: Changes after D-amphetamine. *The Journal of Neurochemistry, 41*(6), 1769–1773.
Zhang, J. C., Lau, P. M., & Bi, G. Q. (2009). Gain in sensitivity and loss in temporal contrast of STDP by dopaminergic modulation at hippocampal synapses. *The Proceedings of the National Academy of Sciences of the United States of America, 106*(31), 13028–13033.